Graduate School ETD Form 9
(Revised 12/07)

PURDUE UNIVERSITY
GRADUATE SCHOOL
Thesis/Dissertation Acceptance

This is to certify that the thesis/dissertation prepared

By Sepehr Farhand

Entitled
Probabilistic Multi-Compartment Deformable Model, Application to Cell Segmentation

For the degree of Master of Science

Is approved by the final examining committee:

Dr.Gavriil Tsechpenakis
Chair

Dr.Shiaofen Fang

Dr.Mihran Tuceryan

To the best of my knowledge and as understood by the student in the *Research Integrity and Copyright Disclaimer (Graduate School Form 20)*, this thesis/dissertation adheres to the provisions of Purdue University's "Policy on Integrity in Research" and the use of copyrighted material.

Approved by Major Professor(s): Dr.Gavriil Tsechpenakis

Approved by: Dr.Shiaofen Fang 04/05/2012
Head of the Graduate Program Date

Graduate School Form 20
(Revised 9/10)

PURDUE UNIVERSITY
GRADUATE SCHOOL

Research Integrity and Copyright Disclaimer

Title of Thesis/Dissertation:

Probabilistic Multi-Compartment Deformable Model, Application to Cell Segmentation

For the degree of Master of Science

I certify that in the preparation of this thesis, I have observed the provisions of *Purdue University Executive Memorandum No. C-22,* September 6, 1991, *Policy on Integrity in Research.**

Further, I certify that this work is free of plagiarism and all materials appearing in this thesis/dissertation have been properly quoted and attributed.

I certify that all copyrighted material incorporated into this thesis/dissertation is in compliance with the United States' copyright law and that I have received written permission from the copyright owners for my use of their work, which is beyond the scope of the law. I agree to indemnify and save harmless Purdue University from any and all claims that may be asserted or that may arise from any copyright violation.

Sepehr Farhand

Printed Name and Signature of Candidate

04/05/2012

Date (month/day/year)

*Located at http://www.purdue.edu/policies/pages/teach_res_outreach/c_22.html

PROBABILISTIC MULTI-COMPARTMENT DEFORMABLE MODEL, APPLICATION TO CELL SEGMENTATION

A Thesis

Submitted to the Faculty

of

Purdue University

by

Sepehr Farhand

In Partial Fulfillment of the

Requirements for the Degree

of

Master of Science

May 2012

Purdue University

Indianapolis, Indiana

This work is dedicated to my parents.

ACKNOWLEDGMENTS

I would like to express my deepest and sincere gratitude to my advisor, Dr. Gavriil Tsechpenakis for his excellent guidance, caring, patience and encouragement throughout my Thesis and Graduate studies. His guidance helped me in all the time of research and writing of this thesis. I could not have imagined having a better advisor and a mentor for my graduate study and I eagerly anticipate working under Dr. Tsechpenakis's guidance in the future as I continue my studies.

I also want to thank Dr. Shiaofen Fang and Dr. Mihran Tuceryan for agreeing to be a part of my Thesis Committee.

Thank you to all my friends and well-wishers for their good wishes and support. And most importantly, I would like to thank my family for their unconditional love and support.

TABLE OF CONTENTS

LIST OF FIGURES

ABSTRACT

Farhand, Sepehr M.S., Purdue University, May 2012. Probabilistic Multi-Compartment Deformable Model, Application to Cell Segmentation. Major Professor: Gavriil Tsechpenakis.

A crucial task in computer vision and biomedical image applications is to represent images in a numerically compact form for understanding, evaluating and/or mining their content. The fundamental step of this task is the segmentation of images into regions, given some homogeneity criteria, prior appearance and/or shape information criteria. Specifically, segmentation of cells in microscopic images is the first step in analyzing many biomedical applications. This thesis is a part of the project entitled "Construction and profiling of biodegradable cardiac patches for the co-delivery of bFGF and G-CSF growth factors" funded by National Institutes of Health (NIH). We present a method that simultaneously segments the population of cells while partitioning the cell regions into cytoplasm and nucleus in order to evaluate the spatial coordination on the image plane, density and orientation of cells. Having static microscopic images, with no edge information of a cytoplasm boundary and no time sequence constraints, traditional cell segmentation methods would not perform well. The proposed method combines deformable models with a probabilistic framework in a simple graphical model such that it would capture the shape, structure and appearance of a cell. The process aims at the simultaneous cell partitioning into nucleus and cytoplasm. We considered the relative topology of the two distinct cell compartments to derive a better segmentation and compensate for the lack of edge information. The framework is applied to static fluorescent microscopy, where the cultured cells are stained with calcein AM.

1. INTRODUCTION

The development of organized vascular networks requires a series of highly specific interactions between cells, growth factors and soluble mediators. Among the various approaches to promote vascular regeneration, therapeutic angiogenesis based on the delivery of soluble cytokines has generated considerable interest because of its minimal invasiveness and promising pre-clinical success. Guided therapeutic angiogenesis (i.e. patterned vascular networks) is possible by controlling the spatial and temporal presentation of soluble mediators at the site of ischemia. By designing nanofibrous scaffolds that direct the local gradients of angiogenic cytokines we could manipulate the proper migration of cells that presages vascular patterning.

The aim of this project is to develop a discriminative semi-supervised multitask learning framework for mixed categorical and numerical observed data, allowing for the prediction of the biological effect of the growth factor releasing constructs as a function of fabrication parameters. Input parameters on our model will include growth factor concentration, type of growth factor (i.e. bFGF alone, G-CSF alone, or G-CSF+bFGF), and construct fiber orientation and dimensions. Output parameters will include release kinetics of the growth factors, cell proliferation, capillary sprouting and orientation (Figure 1.1). Our mathematical model will be validated in a limb ischemic animal model by assessing the angiogenic effect of selected bFGF/G-CSF releasing matrices.

The output from applying different nanofibrous scaffold architecture (Figure 1.2), along with different types of growth factors on an ischemic limb can be automatically evaluated using computer vision and machine learning techniques. Microscopic images at the site of ischemia after this process (Figure 1.3) are used to assess the

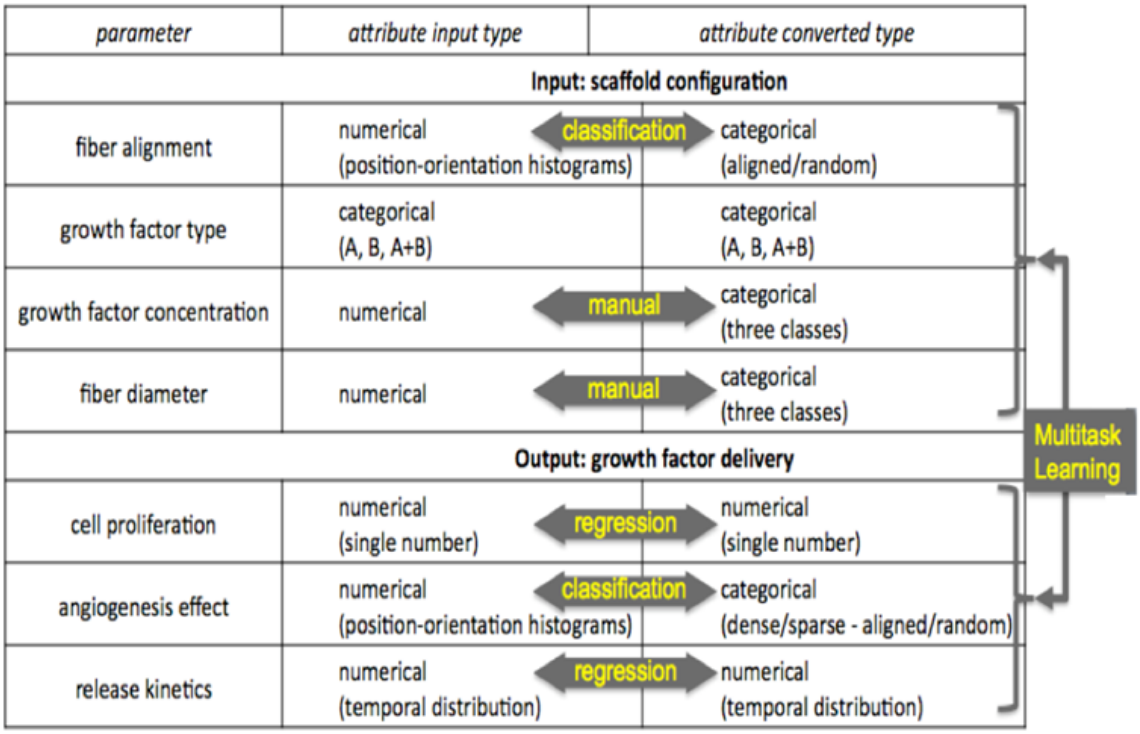

Figure 1.1. Parameter attributes and computational prediction modeling. After the input data are converted into their appropriate form (e.g., fiber orientation histogram into the category aligned or random), using either classification or regression approaches, we will apply a multitask learning framework to model the mapping scaffold configuration growth factor delivery. This modeling will be the system's final prediction module: for any input parameters for the construct configuration (either in the form of the input attributes, or as converted attribute types), we will be able to predict the growth factor delivery, with respect to any of the output parameters (also as either input attribute or converted attribute types). manual indicates the description the growth factor concentration for example, set as low, medium, or high. A and B describe growth factors bFGF and G-CSF.

population, orientation and density of cells. Our objective is to design an algorithm compute desired factors from provided images.

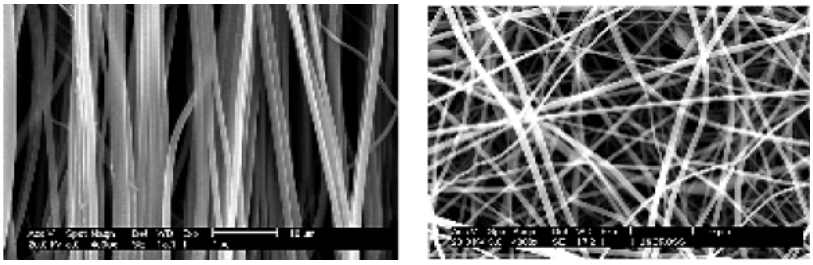

Figure 1.2. Different types of scaffold architecture. The image on the left side is aligned architecture and the right hand side shows the randomly aligned architecture.

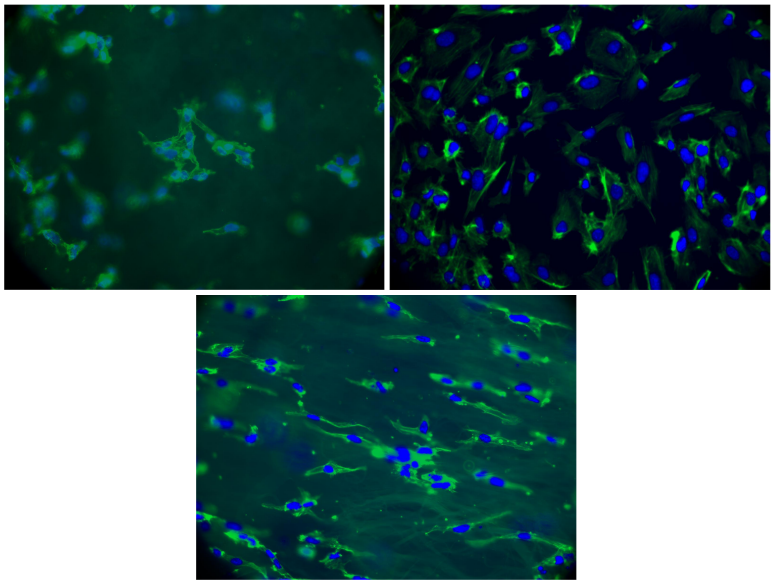

Figure 1.3. Microscopic images at the site of ischemia after the proposed treatment.

1.1 Cell segmentation

Cell segmentation has been the area of attention for many researchers dealing with biomedical applications. The main approaches to address this problem were deformable models and graph cuts. Wang *et al.* [1] use texture adaptive geodesic active contours to bypass internal pseudo-edges and stop on low contract boundaries.

In another work [2] they use Adaboost [3] algorithm to select discriminative features of the image which finds the approximate location of each cell. Using the results from previous step and another set of features (image gradients, intensities and etc.), they train an Support Vector Machine (SVM) [4] to find the foreground. Finally they apply watershed [5] algorithm in the foreground areas to get each individual cell. The databases used in these papers contain monochromic images with good texture information.

As another deformable model approach, Ali *et al.* [6] use geodesic active contours also known as level set deformable models to segment brightfield image cell segmentation. The evolution energy function in this method depends on the smoothness of the curve, difference between curve orientation and the image orientation, and consistency of phase map on zero level-set. Sample images in this work also have relatively good contrast information around cells. Other approaches based on deformable models are [7, 8].

The solution we describe here differs from the existing literature in that (i) we aim at segmenting cells in static images, without considering any temporal changes; (ii) most methods in the literature process grayscale microscopic images, while in our approach we exploit RGB information; (iii) we consider topology constraints of the cell structure for better segmentation; (iv) we integrate region classification with a geometric model; (v) we handle local feature variations by both updating the model interior statistics and employing nucleus membrane relative topology constraints.

Our goal is to model the cell morphology, i.e., extract shapes and relative topology of nucleus and membrane. This is to assess the effect of biologically responsive scaffolds that deliver multiple angiogenic cytokines and/or cells in ischemic regions [9].

We develop an algorithm, which segments cells from microscopic images of vascular networks in an unsupervised learning manner. Geometric deformable model techniques are employed in this thesis since they are the most effective methods in medical image analysis. Having the shape of the target objects not being fixed and in order to capture the uncertainty of our final model, probabilistic deformable model framework is the most suitable choice. In this framework, our knowledge of the shape and membrane-nucleus topology is incorporated in the *a priori* term.

The input of this method is a set of microscopic images in which nucleus and cytoplasm regions are manually stained. Given proposed biomedical process, the output images can be categorized into three different classes: Aligned, Barewell and Random, which defines the orientation of vascular networks (Figure 1.4).

Each cell has two compartments: nucleus and cytoplasm (Figure 1.5). The nucleus region (the blue area) has good edge information and high contrast with respect to the rest of the image. In addition, an eclipse can model the shape of the nucleus region. Thus, segmenting nucleus can be done easily and it can be used to find the location of the cell in the image. On the other hand, cytoplasm region (the bright green area) lacks edge information with no shape constraints and cannot be segmented using traditional image segmentation techniques (Figure 1.6). By considering the above-mentioned properties of the nucleus and the cytoplasm regions, we can reassure that the nucleus region can be used as a solid foundation for finding the cell and controlling the segmentation of the cytoplasm region. Using the result of cell segmentation, the cell alignment will be computed.

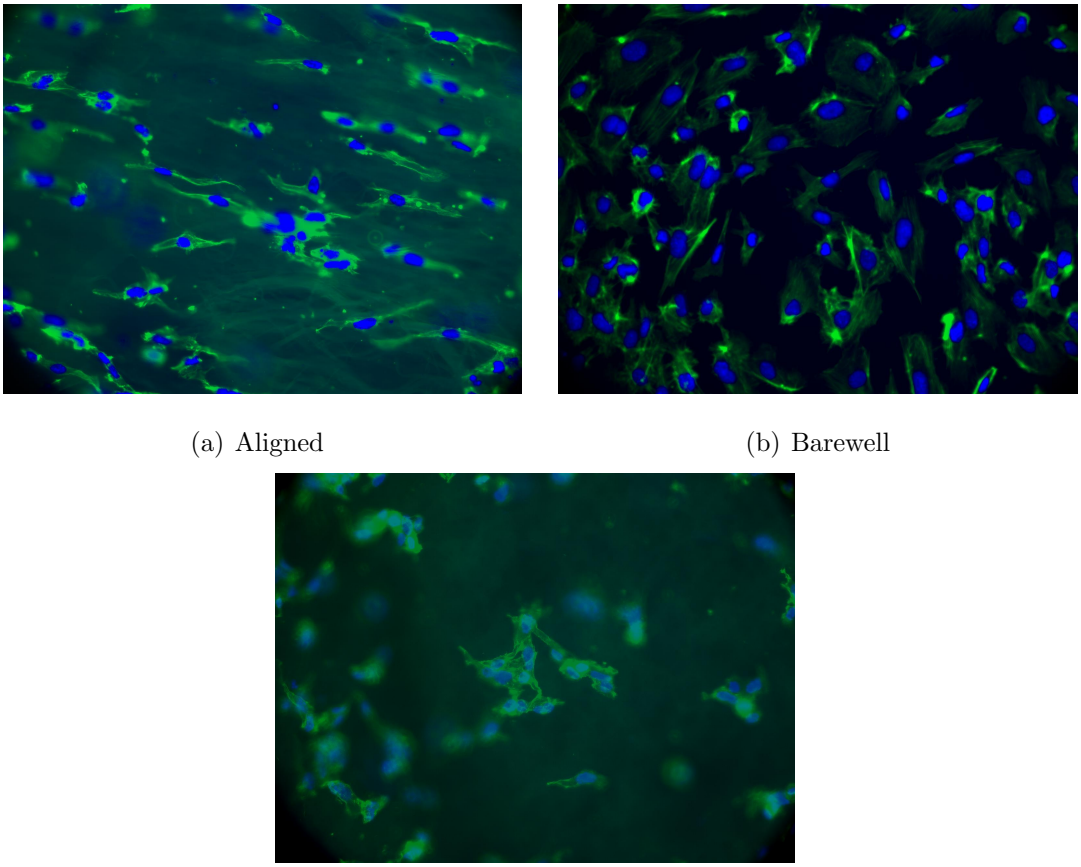

(a) Aligned (b) Barewell

(c) Random

Figure 1.4. Dataset sample images.

Future work on this project would include evaluating the orientation of a vascular network automatically from the segmentation output of these microscopic images and implementing a learning algorithm to define a mapping between the input and the output.

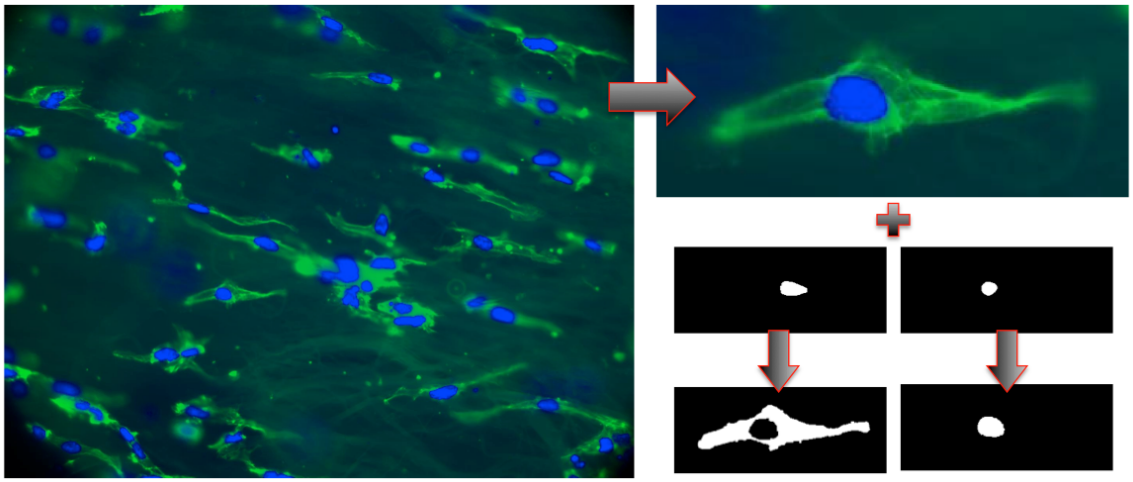

Figure 1.5. Given a microscopic image of cells and annotated seeds in nucleus and membrane, our goal is to segment each of the cells while preserving their structure. Our algorithm runs on an approximate window with two seeds and, after the termination of the deformable model evolution, the algorithm returns two regions, nucleus and membrane, in the approximate window.

Our method extracts individual cells from each image and using the provided stained regions, it evolves nucleus and membrane segments simultaneously. The method returns a nucleus and a membrane mask for the image after the convergence. Each mask represents the corresponding segmented region (Figure 1.5).

The rest of this thesis gives some background on traditional image segmentation techniques, introduces previous works on cell segmentation, our methodology to solve the problem and a brief summary of this work.

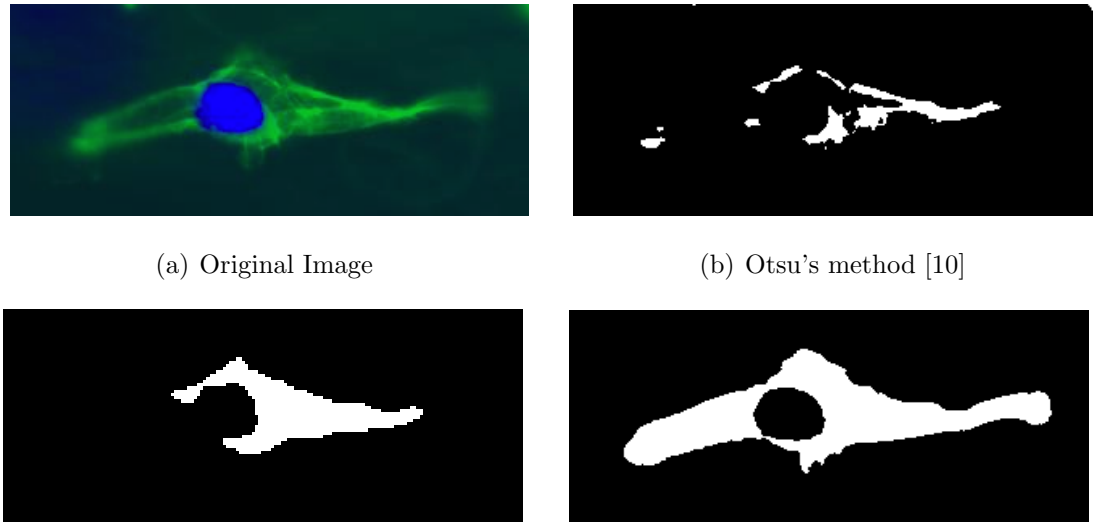

(a) Original Image

(b) Otsu's method [10]

(c) Chan-Vese Segmentation [11]

(d) Our approach

Figure 1.6. A comparison between cytoplasm segmentation of a cell using traditional methods and our approach.

2. BACKGROUND

"The rapid progress in computerized medical image reconstruction, and the associated developments in analysis methods a computer-aided diagnosis, has propelled medical imaging into one of the most important sub-fields in scientific imaging" (Dougherty, [12]). There are many applications of medical image processing and this number is growing. This field has enabled scientists to automatically investigate the affects of different medical experiences over time. Processing digital images in an automatic manner enables us to analyze large amounts of data in a short time relative to employing human experts.

Image segmentation highly affects the content extraction process and it also plays an important role in human visual perception. [13] defines the purpose of segmentation as to decompose the image into smaller regions for further analysis. It can also be defined as finding regions of images that are coherent. A segmented image is normally used as the base data of many pattern recognition or classification tasks. Many approaches have been proposed to accommodate this task i.e. mean shift, graph-based techniques, feature space clustering, etc. Different approaches are used depending on the characteristics of the problem to be solved.

Here, some traditional image segmentation techniques, which segment the input image into different classes, are briefly discussed:

Thresholding is the most trivial method in image segmentation. The main process of this technique is to define a threshold and compare pixels to this value. If the pixel values are higher than this threshold, they will be considered as foreground and otherwise they would be classified as background. This can be done by defined a global

threshold for the whole image and find the optimal value for it which would be done through Otsu thresholding by maximizing the between-class variance [10]. Another method to find this optimal value is "maximum entropy thresholding" which is similar to Otsu's method and it maximizes the between-class entropy [14]. In the case of more than two classes, the Otsu's method can be extended to the multi-thresholding technique.

In some images, it is not possible to compute a single global threshold for the whole image in order to get an optimal segmentation. This can easily happen where we have different non-homogeneous background. To cope with this issue, we can use the "local adaptive threshold" method which divides the image into subregions and applies the mentioned thresholding technique to each region.

Thresholding, in order to acquire a good segmentation result, has a small set of applications and cannot be applied to complex problems.

Edge-based methods try to find regions enclosed by boundaries made of edges. The first step is to find the edges of the image using gradient operators. Since the results from a gradient operator could have discontinuity, there should be some heuristics to find the relation between detected edges and how to they connect with each other to construct a closed boundary. There have been some studies over these heuristics and the results are moderate [15, 16]. In the absence of edge information, noise and background complexity, these methods are not reliable and could not deliver optimal segmentation results. Therefore, Region-based methods which are more robust have been introduced.

The objective of the region-based method is to segment an image into connected regions which have the most inner-region similarity rather than depending on the edge information from the image. Region-based segmentation can be performed un-

der region growing framework. Region growing is a bottom-up approach and used to implement different techniques of image segmentation as well as region-based segmentation. This method starts with an initial estimate of the region of interest and at each step, it adds region's neighboring pixels to this region based on the similarity to the pixels inside of the region. Having more than one seed and growing all of them at the same time requires a mechanism to merge seeds that are similar to each other.

Region-based techniques are suitable for the cases edge information is lacking in the image. They are particularly useful with images which have multi-modal histograms [12].

There exist other segmentation approaches that employ both region-based and edge-based methods:

2.1 Appearance-Based Methods

This family of segmentation techniques is usually based on the statistics of different regions in the image. i.e. watershed [5] segmentation method segments an image into several catchment basins, which are the regions of an image (interpreted as a height field or landscape) where rain would flow into the same lake [17]. There are also a wide range of probabilistic classification approaches based on appearance-based methods.

For example, Wang *et al.* in [2] at one step use wavelet filters to extract the dots corresponding to proteins in the cell nucleus and possible edges relative to membrane edges. Then he uses Adaboost [3] to choose the best features among the result of this filter and finds the cell centers. To find the cell region he trains an SVM [4] based on intensity, gradient and LBP over the whole image. This method cannot be applied in our work context for three reasons: (1) The first step of this method is majorly

dependent on the white halo around the membrane and our dataset does not accommodate a vivid boundary around the membrane 2.1. (2) The second step is based on trained SVM over the whole image and in our case, different images would have different intensities over the dataset which we cannot train a normal SVM for the whole dataset, not to mention the bleaching of parts of images. (3) This method requires modest user interaction to define positive and negative areas which we intend to avoid.

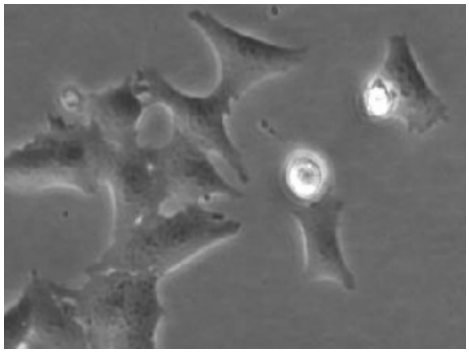

Figure 2.1. A sample of input image in Wang *et al.* problem [2].

Yin *et al.* in [18] use a bag of local Bayesian classifiers that trains a set of local classifiers from image patches and saves them with their corresponding local histograms. To classify a new pixel, this method calculates the local histogram around the pixel and applies weight to each classifier based on similarity of classifier's histogram to the pixel's histogram. Using this method, a soft classification will be applied to each individual pixels of a new test image. This method may lead to sharp edges, unconnected membrane region or holes in our final results. Furthermore, it needs accurate annotated data for every possible situation and intensity of a microscopic image. Bleaching, changes in the intensity of our colored dataset and adding another class to the method introduced, might lead to indeterminable results.

Although appearance-based methods take into account the homogeneity constraints and model statistics, they don't constrain the solution model. This weakness can be resolved using deformable models.

2.2 Deformable Models

Deformable models are powerful model-based techniques, which are widely used in image analysis tasks. They exploit (bottom-up) constraints derived from the image data together with (top-down) a priori knowledge about the location, size, and shape of these structures [19]. Having a priori knowledge in these techniques gives them the flexibility of interacting with experts' knowledge in medical image analysis. Internal and external forces and constraints control deformable models. These elastic bodies should minimize the deformation energy function. This deformation energy function is a combination of smoothness, shape information and constraints.

2.2.1 Parametric deformable models

Snakes or "deformable contour models" are a subcategory of deformable models proposed in [20] by Kass *et al.*. "Snakes are two-dimensional generalization of the 1D energy-minimizing splines" (Szeliski, [17]), which define a boundary around the region of interest (ROI). If $(x, y)^T$ is a point on Cartesian coordinates of the image plane (Ω), the parametric curve on this system is defined by $v(s) = (x(s), y(s))^T$ which is parameterized by $s \in [0, 1]$. The energy function defined for this contour is:

$$E^*_{snake} = \int E(v(s))ds = \int U(v(s)) + P(v(s))\ ds\ , \tag{2.1}$$

where E^*_{snake} is the energy of the curve and $U(v(s))$ corresponds to the internal energy of the contour that controls the tension and rigidity [20]. The second term on the right hand side, $P(v(s))$, corresponds to the external energy of the contour and minimization of which forces the contour towards the desired image features. If

P(v(s)) and S(v(s)) are defined as in [20], the Euler-Lagrange equation for the energy term E is:

$$\frac{\partial E^*_{snake}}{\partial s} = 0 \tag{2.2}$$

$$-\frac{\partial}{\partial s}(w_1\frac{\partial v}{\partial s}) + \frac{\partial^2}{\partial s^2}(w_2\frac{\partial^2 v}{\partial s^2}) + \nabla P(v(s,t)) = 0 \ , \tag{2.3}$$

where this equation introduces a balance between the internal and external forces.

Probabilistic deformable models have been introduced by Szelisti [21]. In this framework the solution can be seen as a model fitting process. Furthermore, it allows a measure of the uncertainty in the estimated shape parameters [19]. If we consider u as the shape parameter and I as the observation, we can model the problem as:

$$p(u|I) = \frac{p(I|u)p(u)}{p(I)} \ , \tag{2.4}$$

where $p(u)$ is the prior knowledge of the parameters which stands for the internal energy (smoothness, shape and etc.). $p(I|u)$ is the imaging model which represents the imaging model (external energy).

2.2.2 Geometric deformable models

Level-set methods introduced by Osher *et al.* [22] have been used in deformable models extensively. In these methods, the evolving curve divides the image domain Ω into region R_C enclosed by the curve C and the background $\Omega \backslash R_C$ [23]. The model shape is represented implicitly by its distance transform,

$$\Omega_C(\mathbf{x}) = \begin{cases} 0, & \mathbf{x} \in C \\ +min_{\mathbf{x}\in C}||\mathbf{x} - \mathbf{x}_C||, & \mathbf{x} \in R_C \\ -min_{\mathbf{x}\in C}||\mathbf{x} - \mathbf{x}_C||, & \mathbf{x} \in \Omega \backslash R_C \end{cases} \ , \tag{2.5}$$

where $\mathbf{x} = (x, y)$ is the image pixel location in Cartesian coordinates. The level-set function, $\phi(x, y, t)$ changes over time to accommodate the evolution of the zero level-curve. The evolution in general form is presented as:

$$\frac{\partial \phi(x, y, t)}{\partial t} = F|\nabla \phi| \ , \tag{2.6}$$

where F is the speed of the evolution process which moves the zero level-curve normal to the curve. Corresponding deformable model and its propagation direction is shown in Figure 2.2.

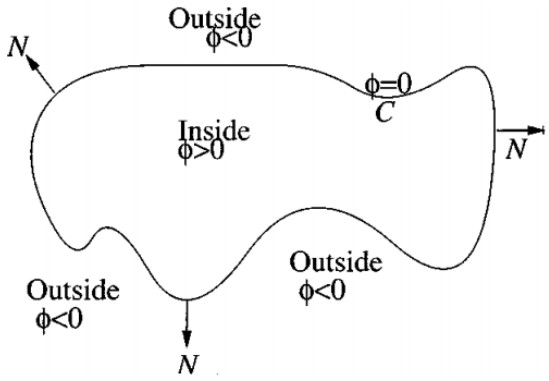

Figure 2.2. Deformable model and its propagation.

In [11], Chan *et al.* use this method with region-based active contours. Their framework does not depend on the edge information of the image and tries to minimize the inner class variance. This criteria makes this technique and it's derivatives i.e. probabilistic level set contours suitable for images with bad edge information. In the following we describe some works done using geometric deformable models.

In [1], Wang *et al.* use texture-adaptive geodesic active contours. This solution proposed by [1] rely on the distinct texture of the image around the membrane bound-

ary as in [2]. Since this information is not available in our problem, this work cannot be applied to our situation.

In [24], a new deformable model is introduced named front vector flow guided active contour. In this work, the regions located between the cell centers and the cell boundary is homogeneous causing minimum energy for front vector flow at the membrane boundary. This is mainly impacted by the intensity differences at the boundary of membrane. This method also cannot be used in our problem due to the lack of rapid intensity changes in our dataset.

In the work of [8], shape prior information and a new edge detection method is incorporated in a level-set framework. Shape prior information is applied by a given set of reference shapes and it is assumed that the final deformable model would have a combination of these shape priors. This clearly cannot be applied to our dataset because of different orientation, shape and size of each cell membrane and also non-satisfactory results on our colored high quality samples (Figure 2.3).

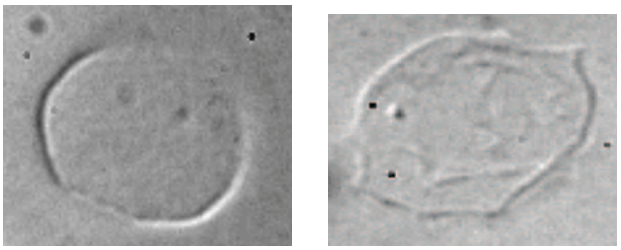

(a) Sample 1 (b) Sample 2

Figure 2.3. Sample input images from Chen *et al.* paper. As it can be seen, the shape of the target object has a low variance over the dataset.

In [25], cell segmentation is done using a combination of appearance-based techniques and deformable models. This method estimates the spatial intensity distri-

bution of nucleus as a Gaussian model and uses level-set method to find the cells in an image. This method does not work for us because we would like to segment membrane, which cannot be presented as a Gaussian model. Moreover, this method assumes a constant intensity background, which in our case the background's intensity varies and it might overlap with cell intensity values. This would cause numerous false positives in our dataset.

This thesis draws motivation from the paper by Tsechpenakis and Metaxas [26] which describes mechanism of using an implicit deformable model driven by Conditional Random Fields (CRFs) [27] to perform topology independent. They define a simple graphical model representing the problem and achieve the optimal solution for the deformable model by Maximum A Posteriori estimation. In this thesis we extend the work of Tsechpenakis *et al.* by using the *a priori* knowledge on ROI structure which allows the evolution of membrane and nucleus in a simultaneous manner.

3. METHODOLOGY

In our proposed method we combine the region-based geometric models, the graphical models and the structural information of cells. Here we refer to structure as the relative position of nucleus with respect to cytoplasm (relative topology). We build a simple graphical model to solve the joint evolution of two interfaces, namely the nucleus and membrane boundaries (Figure 3.1). Since the two compartments are stained in blue and green respectively and red channel does not contribute any information about these compartments, we consider green and blue channels to decompose the input RGB image. Initially, we use the manually stained regions to detect the pixels that are more likely to belong to each compartment. For this purpose, we use K-harmonic means clustering (KHM) [28] with $K \geq 3$, to over-segment the data and calculate the highest pixel memberships to the nucleus and cytoplasm compartments. During evolution, we update the probability field based on the new model position, which enables us to capture local intensity inhomogeneity in the two compartments.

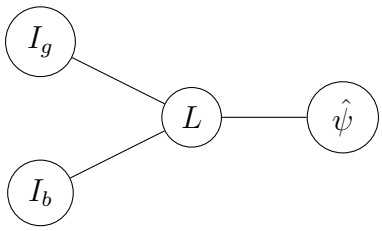

Figure 3.1. Integration of shape, relative topology, and region classication in a probabilistic graphical model.

Let x be a pixel location with Cartesian coordinates (x_1, x_2) in the image domain Ω and let $I_g(x)$ and $I_b(x)$ be the intensities of the green and blue channel at the pixel

x respectively. Also, let $L = \{l(x)\}_{x\in\Omega}$ be the set of pixel labels on the image plane. The label of each pixel can be achieved using $l(.)$ function:

$$l(x_i) = \begin{cases} 0, & Cytoplasm \\ 1, & Nucleus \\ -1, & Background \end{cases} \tag{3.1}$$

where i is a pixel index in the image plane.

In order to be able to segment the nucleus and membrane simultaneously, we have decomposed the cell shape $\hat{\psi}$ into its compartments ψ_N and ψ_C which are signed distance functions [23] of nucleus and membrane respectively and we define them as:

$$\psi_N(x) = \begin{cases} 0, & x \in M_N \\ +d(x, M_N), & x \in R_N \\ -d(x, M_N), & x \in \Omega\backslash R_N \end{cases} \tag{3.2}$$

where R_N is the nucleus region with boundaries M_N, and

$$\psi_C(x) = \begin{cases} 0, & x \in M_C \\ +d(x, M_C), & x \in R_C \\ -d(x, M_C), & x \in \Omega\backslash R_C \end{cases}, \tag{3.3}$$

where R_C is the cytoplasm region with boundaries M_C shown in Figure 3.2.

Our solution for the estimation of the desired boundaries is based on the graphical model in Figure 3.1 which shows the association between the evolving interfaces ($\hat{\psi}$), collection of pixel labels (L) and the image space information (I_g, I_b). To capture relative topology, we implicitly consider that the regions of interest are conditionally dependent and do not overlap in the image domain.

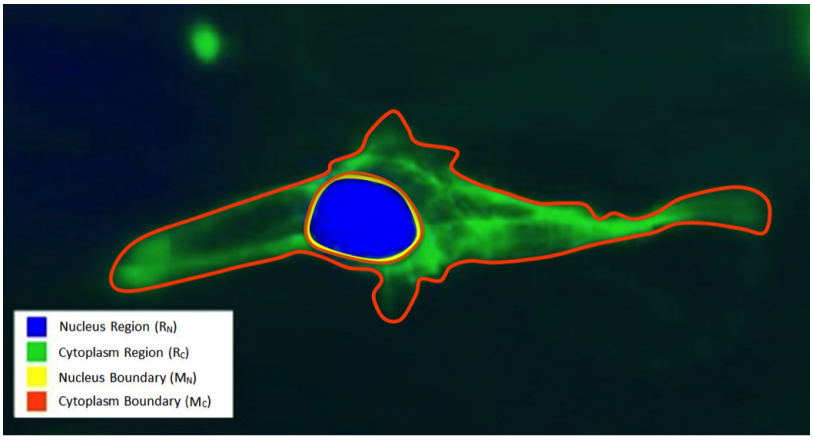

(a) Segmented Cell

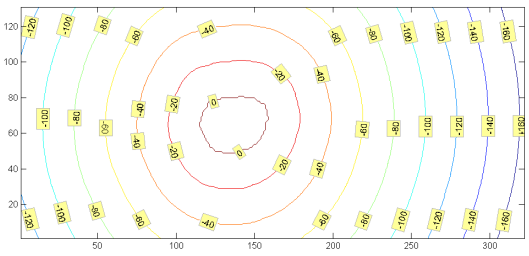

(b) Signed distance function of nucleus

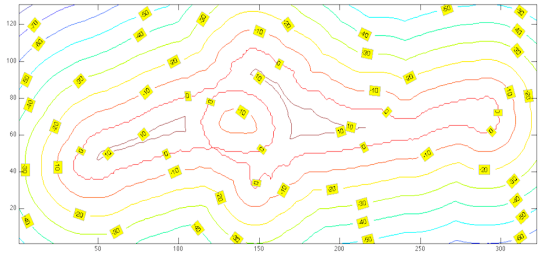

(c) Signed distance function of cytoplasm

Figure 3.2. Illustrating $R_N, R_C, M_N, M_C, \psi_N, \psi_C$.

3.1 Deformable model formulation

Deformable model configuration ($\hat{\psi}$) captures three distinct regions according to appearance and relative topology of the cell compartments. Our proposed method is presented in a probabilistic framework. We would like to maximize the posterior probability of pixel labels and cell deformable model given the image observations:

$$< \hat{\psi}^*, L^* >= \arg\max_{(\hat{\psi}, L)} P(\hat{\psi}, L|\hat{I}) \tag{3.4}$$

Using Bayesian rule we decompose our problem into terms that can be evaluated using our graphical model (Figure 3.1):

$$P(\hat{\psi}, L|\hat{I}) = \frac{P(\hat{\psi}).P(L|\hat{\psi}).P(L|\hat{I})}{P(L)} \tag{3.5}$$

$$\propto P(\hat{\psi}).P(L|\hat{\psi}).P(L|\hat{I}) \tag{3.6}$$

3.2 $P(\hat{\psi})$: Model prior with relative topology

As it has been discussed in section two, $\hat{\psi}$ is decomposed into ψ_N and ψ_C. The reason of treating the deformable model this way is that the nucleus and cytoplasm are topologically dependent and this information can be used in the evaluation process of the deformable model. Therefore, we include this piece of information as a conditional dependency between ψ_N and ψ_C. Using chain rule we have:

$$\begin{aligned} P(\hat{\psi}) &= P(\psi_N, \psi_C) \\ &= P(\psi_N).P(\psi_C|\psi_N) \\ &= P(\psi_C).P(\psi_N|\psi_C) \end{aligned} \tag{3.7}$$

As it can be seen in 3.7, using the chain rule of probability, the general model could decompose into two different forms. The confidence in the nucleus position, due to the shape information and intensity information from the blue channel, is higher than the cytoplasm. Therefore, we can evaluate the shape of cytoplasm using the conditional dependency of the cytoplasm given the nucleus ($P(\psi_C|\psi_N)$). This dependency fits into the last line of equation 3.7.

The following is the definition of nucleus internal energy considering its area $A(R_N)$, smoothness and shape as how perfectly it fits an ellipse.

$$\begin{aligned} E_{int_N} &= \varepsilon_1 A(R_N) \\ &+ \varepsilon_2 \int\int_{\partial R_N} ||\nabla \psi_N(x)|| dx \\ &+ \varepsilon_3 Ellipse(R_N) \ , \end{aligned} \tag{3.8}$$

s.t. $\varepsilon_1, \varepsilon_2$ and ε_3 are constants. Minimizing this energy function should maximize the model prior (Eq. 3.7). ∂R_N defines a narrow band around the nucleus boundary in order to evaluate the smoothness of a local area. For evaluating how perfectly the nucleus fits an ellipse we used [29]. When the nuclei's shape becomes closer to an ellipse, $Ellipse(R_N)$ in 3.9 would converge to zero and the energy function decreases.

$$Ellipse(R_N) = \frac{R_N \cap R_e^*}{R_N \cup R_e^*}, \tag{3.9}$$

where R_e^* is the region enclosed by the ellipse that best ts the nucleus boundaries. The normalized output of this function is shown in Figure 3.4.

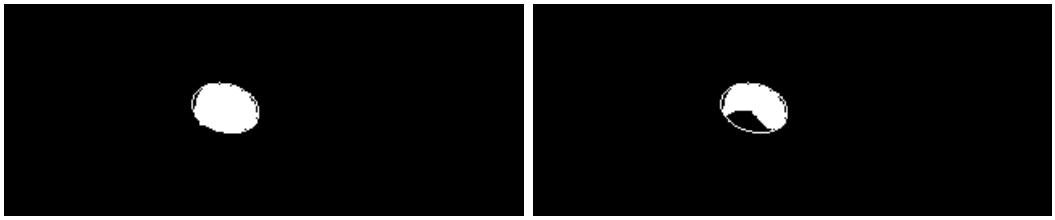

(a) $Ellipse(R_N) = 0.1479$ (b) $Ellipse(R_N) = 0.3298$

Figure 3.3. Outputs of $Ellipse(.)$ function.

Similar to [19, 26, 30], in order to use this energy function in our probabilistic framework, we use Gibbs prior:

$$P(\psi_N) = (\frac{1}{Z_{int_N}})exp\{-E_{int_N}\} \tag{3.10}$$

The equation above is the first part of the model prior in the objective form of equation 3.6:

$$P(\hat{\psi}) = P(\psi_N).P(\psi_C|\psi_N)$$

For the second part of the model prior ($P(\psi_C|\psi_N)$) we define another internal energy function for the cytoplasm area given the nucleus. In order to make use of the topology dependency between cytoplasm and nucleus in a cell, we would like to define a new concept, *joint part*. A joint part is defined between every two adjacent regions (objects) with different labels. For this purpose we used the definition of joint part used in [31]:

Having function $\delta(O)$ returning the boundaries of the object O, if O_i and O_j are two objects sharing a part of their boundary ($O_i \cap O_j \neq \emptyset$) and the shared boundary would be $b_{ij} = \delta(O_i \cap O_j)$ and the boundary of their union would be $B_{ij} = \delta(O_i \cup O_j)$, the joint part of O_i and O_i is defined as:

$$J_{ij} = \{x \in O_i \cup O_j | \min_{y \in b_{ij}} ||x - y|| < \min_{z \in B_{ij}} ||x - z||\} \tag{3.11}$$

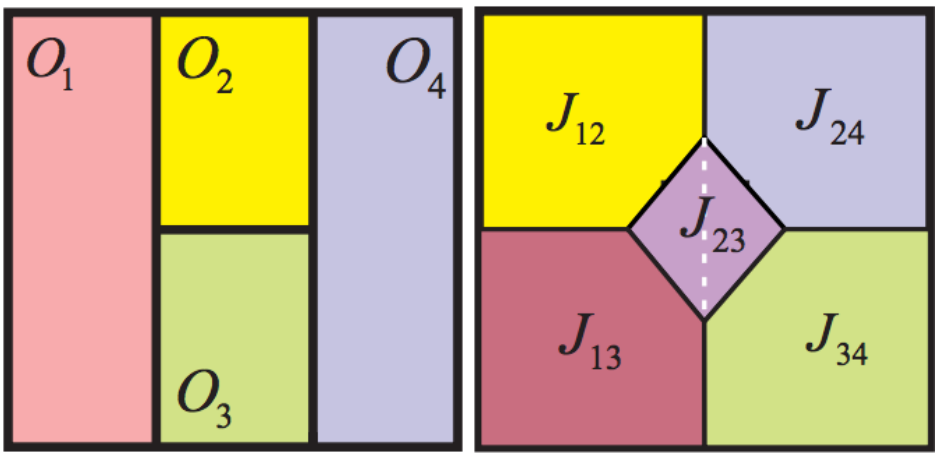

(a) Objects in the image (b) Pairwise joint parts

Figure 3.4. Joint part definition [31].

Also, the notion of the *first neighbor* is introduced to define the label function,

$$f(x) = j, \ if \ x \in O_i \cap J_{ij}, \forall (i,j) \in [1,3], i \neq j, \tag{3.12}$$

i.e.,

$$x \in J_{ij},\ if\ \{l(x), f(x)\} = \{i, j\}\ or\ \{j, i\} \tag{3.13}$$

Finally, the distance,

$$\varphi_f = \sum_{i,j=1, i\neq j}^{3} \max\{\psi_{ij}, 0\} - \max\{\psi_i, \psi_j, 0\}, \tag{3.14}$$

is considered, where ψ_{ij} is the distance function of $O_i \cup O_j$, and $\psi_{i\ or\ j} = \{\psi_N, \psi_C, \psi_B\}$.

Following the definitions above, the topology and shape of the cell can be modeled in the image domain by the functions φ_J and φ_F, and the individual shapes can be recovered by,

$$\psi_i(x) = \begin{cases} \varphi_J, & \text{if } l(x) = i \\ -\varphi_J, & \text{if } l(x) \neq i \text{ and } f(x) = i \\ -\varphi_J - \varphi_F, & \text{if } l(x) \neq i \text{ and } f(x) \neq i \end{cases} \tag{3.15}$$

Figure 3.5 illustrates the joint parts and the boundaries M_N, M_C at three instances (t_1, t_2, t_3) during evolution. Notice that at t_1, the joint part J_{NC} (nucleus-cytoplasm) is empty since the two regions are not adjacent; similarly, for joint part of nucleus-background at t_3, we have $J_{NB} = \emptyset$.

Using these definitions we can define the internal energy function corresponding to cytoplasm as:

$$\begin{aligned} E_{int_C} &= \varepsilon_4 A(R_C) \\ &+ \varepsilon_5 \int\int_{\partial R_C} ||\nabla \psi_C(x)|| dx \\ &+ \varepsilon_6 \frac{A(J_{NB})}{A(J_{NC})}\ , \end{aligned} \tag{3.16}$$

where $\psi_N(x_i)$ and $\varepsilon_4, \varepsilon_5$ and ε_6 are constants. The minimization of this energy, in a similar way as equation 3.9, enforces minimum area and maximum local shape

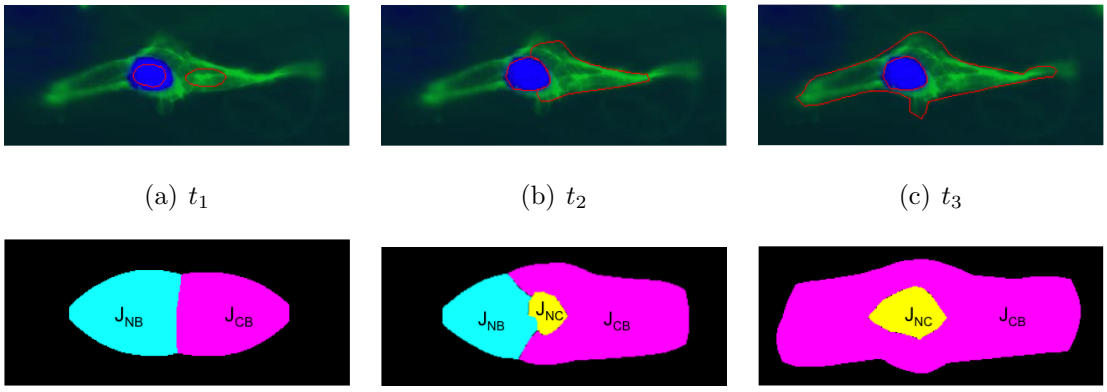

(a) t_1 (b) t_2 (c) t_3

(d) t_1 (e) t_2 (f) t_3

Figure 3.5. Demonstrating the evolution of deformable model on the first row ($t_1 < t_2 < t_3$) and corresponding changes to joint parts on the second row; where J_{NB}, J_{CB} and J_{NC} are nucleus-background, cytoplasm-background and nucleus-cytoplasm joint parts respectively.

smoothness, while last term would attract the cytoplasm pixels to the nucleus region and forces the cytoplasm region to grow around the nucleus region and fill the gap (background) between cytoplasm and nucleus (*i.e.* Figure 3.5(c)). Then, the joint topology likelihood of equation 3.17 is,

$$P(\psi_C|\psi_N) = (\frac{1}{Z_{int_C}})exp\{-E_{int_C}\}, \tag{3.17}$$

where Z_{int_C} is the normalization constant.

3.3 $P(L|\hat{\psi})$: Likelihood of L given the model

Dependency of the shape model and pixel labels is defined as:

$$P(l(x_i) = 1|\hat{\psi}) = \frac{g(\psi_N(x_i))}{g(\psi_N(x_i)) + g(\psi_C(x_i)) + g(-\max(\psi_N(x_i), \psi_C(x_i)))} \tag{3.18}$$

$$P(l(x_i) = 0|\hat{\psi}) = \frac{g(\psi_C(x_i))}{g(\psi_N(x_i)) + g(\psi_C(x_i)) + g(-\max(\psi_N(x_i), \psi_C(x_i)))} \tag{3.19}$$

$$P(l(x_i) = -1|\hat{\psi}) = \frac{g(-\max(\psi_N(x_i), \psi_C(x_i)))}{g(\psi_N(x_i)) + g(\psi_C(x_i)) + g(-\max(\psi_N(x_i), \psi_C(x_i)))}, \tag{3.20}$$

where $g(.)$ is the Sigmoid function.

The above equations calculate the probability of a pixel's label based on its distance to the boundaries of each region. The correctness of this formulation can be shown by considering a pixel in a region O and away from region O's boundaries. In this case, the probability of the pixel belonging to O's adjacent regions is less than the probability of the pixel when it is close to O's boundaries (Figure 3.6).

These equations could also be expressed using Softmax function as follows:

$$P(l(x_i) = 1|\hat{\psi}) = \frac{exp(a_N)}{exp(a_N) + exp(a_C) + exp(a_B)} \tag{3.21}$$

$$P(l(x_i) = 0|\hat{\psi}) = \frac{exp(a_C)}{exp(a_N) + exp(a_C) + exp(a_B)} \tag{3.22}$$

$$P(l(x_i) = -1|\hat{\psi}) = \frac{exp(a_B)}{exp(a_N) + exp(a_C) + exp(a_B)}, \tag{3.23}$$

where $a_N = \psi_N(x_i)$, $a_C = \psi_C(x_i)$ and $a_B = \psi_B(x_i)$ which is the signed distance function of the background defined in a similar way as $\psi_N(x_i)$ and $\psi_C(x_i)$.

3.4 $P(L|\hat{I})$: Probability of regions given the image observations

To estimate this probability term, we define a support vector machine (SVM) [4] which is updated at each step of the deformable model evolution. The feature used in this SVM is image intensity corresponding to each image pixel and the result would

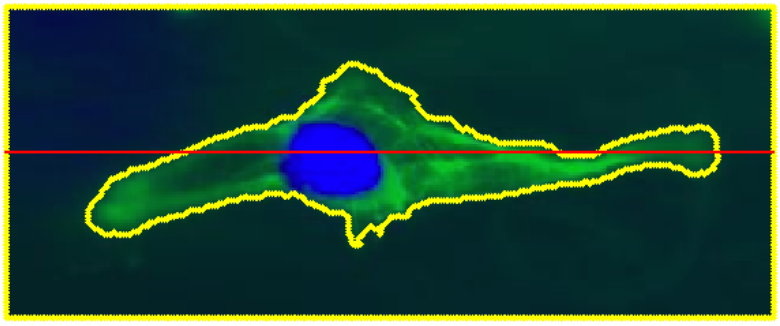

(a) Segmentation of a cell. The boundary of the background is annotated by the yellow lines.

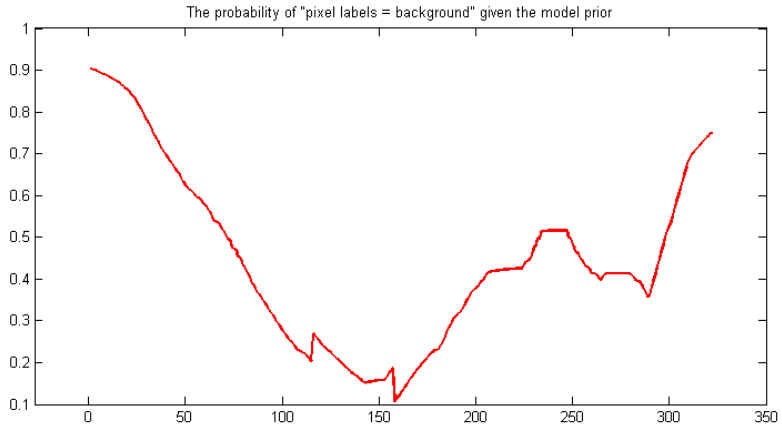

(b) Probability of the pixel labels being background along the red line in 3.6(a).

Figure 3.6. Likelihood of L = "Background" given the model.

be the probability of the pixel belonging to each region. Green and blue channels are the most informative channels in the image space, so we ignored red channel.

$$P(L|\hat{I}) = P(L|I_b, I_g) \tag{3.24}$$

This part of the solution consists of two phases:

3.4.1 Initialization

Initially we apply K-harmonic means clustering [28] on the image intensity feature space with "$k >>$ number of compartments" (for example $K = 7$) to obtain an over-segmentation in this space. This guarantees that we would find at least one cluster for each of nucleus and membrane areas in the intensity space.

Initial nucleus and membrane clusters are chosen are known given annotated seeds. The nucleus and membrane segments from the chosen clusters with the most overlapped region with the nucleus and membrane seeds are added to the corresponding seeds, resulting enhanced seeds for nucleus and membrane. The rest of the image is labeled as background.

3.4.2 Probability field

We train a multi-class support vector machine for this labeled data by employing "one-vs-the rest" method [32]. This method returns one function for each decision boundary.

$$\begin{cases} f_C(\hat{I}_i) \text{ from the SVM with cytoplasm against others} \\ f_N(\hat{I}_i) \text{ from the SVM with nucleus against others} \\ f_B(\hat{I}_i) \text{ from the SVM with background against others} \end{cases},$$

where $\hat{I}_i$ is the blue and green intensities of the pixel i. We use the Sigmoid function [33] to convert the outputs of these functions into probabilities.

$$P(l_i = y|\hat{i_i}) = \frac{1}{1 + exp(-f_y(\hat{i}_i))} , \tag{3.25}$$

where $y \in \{-1, 0, 1\}$. After each step of the deformable model evolution, updated information about the pixel labels are used to update SVM. Updated support vector

machine is used in the Sigmoid function defined above (equation 3.25) at the next step of posterior probability estimation of labels given the image intensities.

3.5 Finding approximate windows

The proposed probabilistic model can be applied on one cell at a time. In this section we explain how we can use this model to perform the segmentation on the original image. The goal of approximate window is to find an approximate window around a cell with initial seeds for nucleus and membrane and apply the segmentation model in that window.

We start by applying K-harmonic means on the pixel intensities with $K = 7$ in order to find initial reliable clusters for nucleus and membrane. We use annotated seeds to find clusters corresponding to each region. The clusters with the most number of nucleus and membrane seed pixels are labeled as nucleus and membrane clusters respectively (Figure 3.7).

Due to the high contrast of the nucleus area in our dataset, we can use this area to find approximate windows for each cell. We know that the nucleus is the heart of a cell. We want one nucleus in each window and the goal is to have this window to be as large as possible to contain the whole structure of a the nucleus's cell while avoiding to include other cells' components. This window can be achieved by starting from the centroid of each nucleus and expand a square window around it. Each side of this growing window will move with the speed = 1 and normal to itself. Each side will stop moving when it reaches a neighboring nucleus. The evolution of the square is implemented using morphological operations. Once all of the sides are fixed, the approximate window is achieved (Figure 3.8).

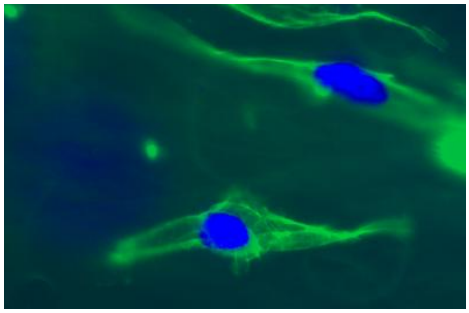

(a) Original Image

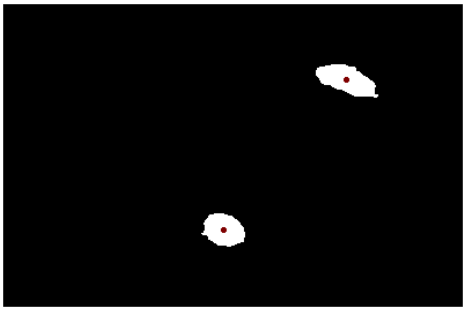

(b) Nucleus Cluster

(c) Membrane Cluster

Figure 3.7. Intensity clusters selected for each compartment using annotated seeds. Centroids of the nucleus segments are marked with red circles.

Each approximate window contains one nucleus segment and multiple membrane segments. The membrane segment which is the closest one to the nucleus in each approximate window will be selected as the initial membrane seed. (Figure 3.9)

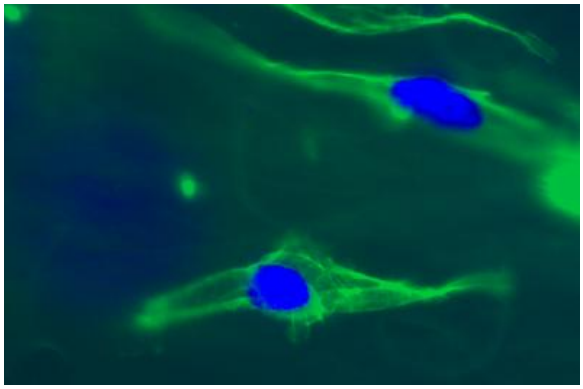

(a) Original Image

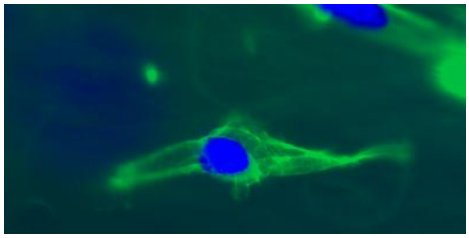

(b) Approximate window for cell # 1

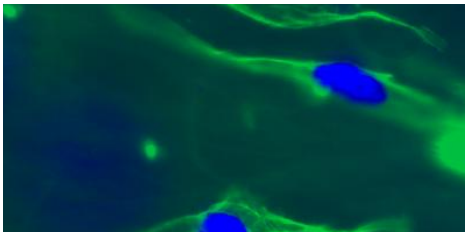

(c) Approximate window for cell # 2

Figure 3.8. Approximate windows selected for an image containing two cells.

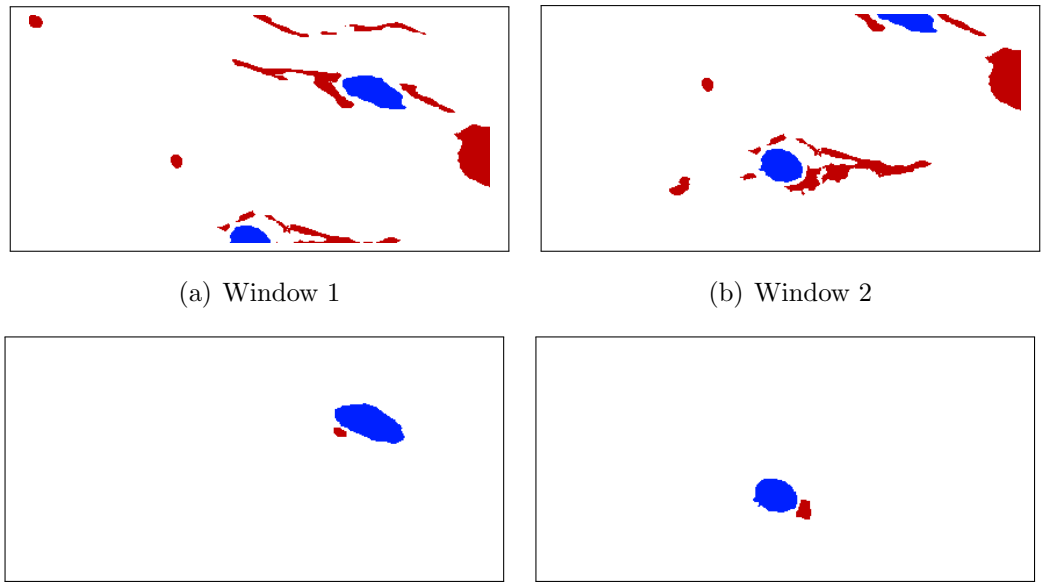

(a) Window 1

(b) Window 2

(c) Window 1 seeds

(d) Window 2 seeds

Figure 3.9. Initial seeds in each window. The top row shows each window with multiple membrane segments. The bottom row shows the selected seeds for membrane and nucleus in each approximate window.

4. RESULTS

We applied our method on a set of 20 single cell images cropped from the original dataset provided by bioengineering department at University of Miami. All experiments were performed on a MAC PRO computer with 3.2 Ghz Quad-Core Intel Xeon and 12 GB of memory. Performing segmentation on each image takes 10-20 minutes dependent upon the employed over-segmentation method. As it has been discussed in previous chapter, simultaneous segmentation of cells in an image can be done using approximate window and applying the proposed model on each of these windows.

Figures 4.1 and 4.2 show the result of our segmentation method. In some cases with minimum photo-bleaching, the initialization for the nucleus and/or membrane regions is very close to the desired boundaries. Therefore, to show the scalability of our approach, we manually chose seeds among the regions that are initially assigned to corresponding classes by the K-harmonic means clustering.

In all examined images, our model correctly captures $> 97\%$ of the nucleus, with $< 2\%$ of its area false positive assignments, and $> 91\%$ of the membrane, with $< 4\%$ of the its area false positives. Due to the topology constraints we imposed between the two compartments, during evolution the estimated membrane region does not leak at the sites where the photo-bleaching degree is high.

The choices of the weight parameters in equations 3.9 and 3.17 directly affect the effectiveness and accuracy of our model. Since the main forces deriving the cell model are from the ellipse fitting term in equation 3.9 and the joint topology term in

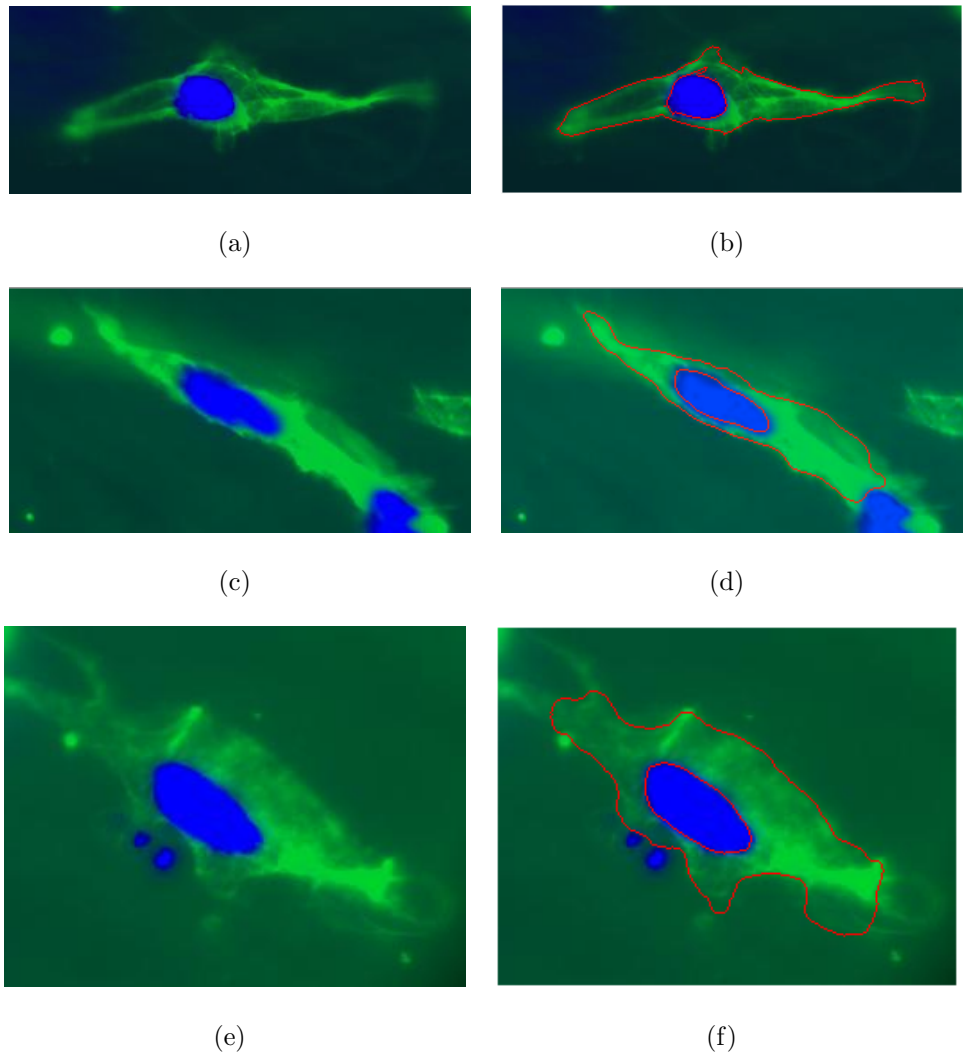

(a) (b)

(c) (d)

(e) (f)

Figure 4.1. Segmentation results with normalized cuts over-segmentation. Original images on the left hand side, segmented results on the right hand side.

equation 3.17, the weights corresponding to these two terms (ε_3 and ε_6) are assigned higher values in cases of increased noise. In most of our experiments the choice of the parameters were $\{\varepsilon_1, \varepsilon_2, \varepsilon_3, \varepsilon_4, \varepsilon_5, \varepsilon_6\} = \{0.2, 0.3, 0.5, 0.3, 0.1, 0.6\}$.

In general, different initialization methods could result in different segmentations with different accuracies. We claim that using an initialization method, which would

return a true over-segmentation of the image space, our method can find the optimal segmentation of the cell image. We have applied two different over-segmentation methods in our experiments: Normalized cuts segmentation (N-cuts) [34] and K-harmonic means clustering. In 4.1(f), a part of background is segmented as cytoplasm due to the under-segmentation of the normalized cuts segmentation method in this image. This problem will be resolved by changing the input parameters of the normalized cuts segmentation method in order to obtain the true over-segmentation of the cell image.

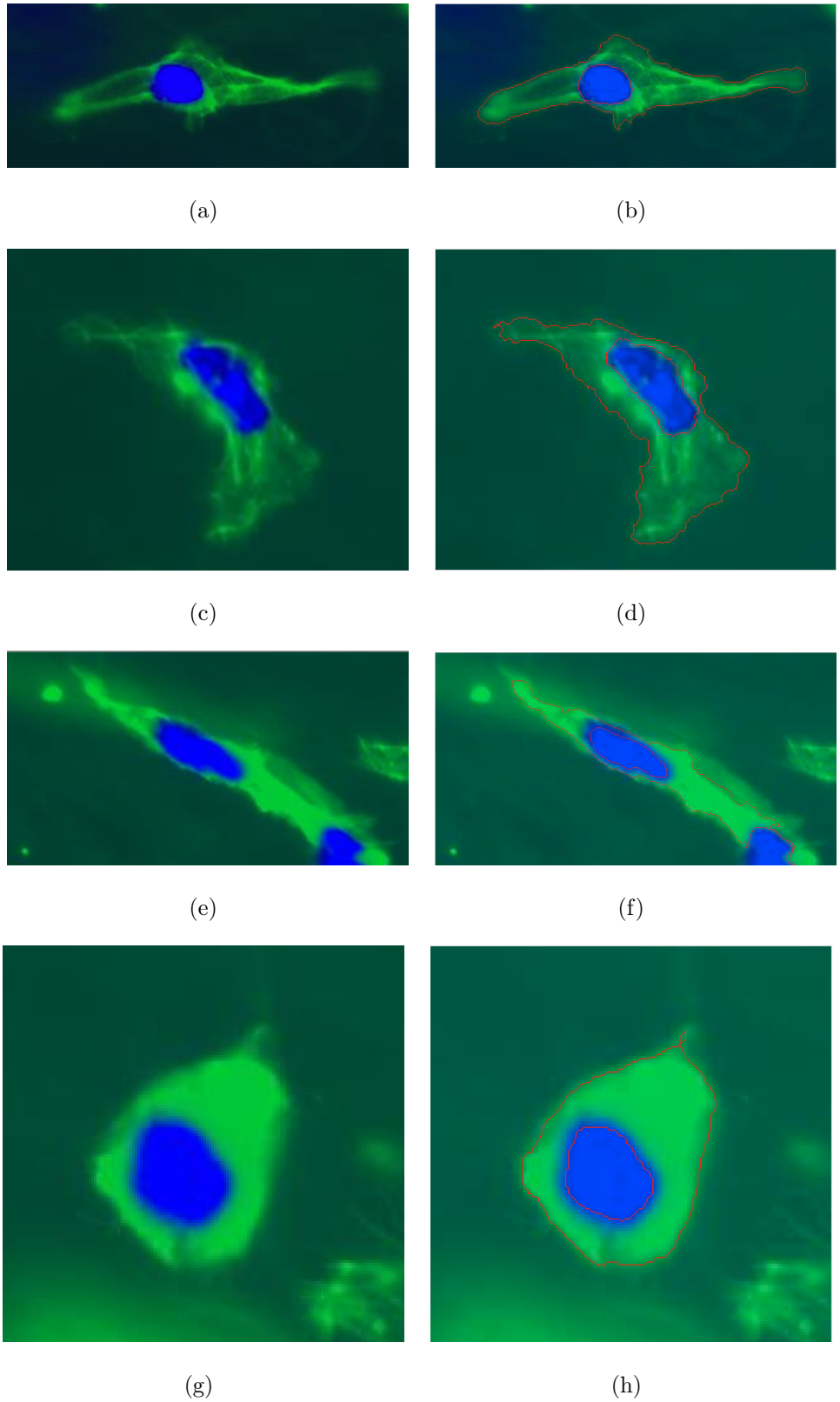

(a) (b)

(c) (d)

(e) (f)

(g) (h)

Figure 4.2. Segmentation results with K-harmonic means over-segmentation. Original images on the left hand side, segmented results on the right hand side.

5. SUMMARY

In this thesis we presented a probabilistic geometric deformable model that simultaneously segments the compartments of an object using the relative topology of compartments with respect to each other. We applied this method to the problem of segmenting cell populations in order to segment the nucleus and the cytoplasm regions of this population. This model captures the relative topology of the cell and manages to perform well on our test data, which lacks edge information.

The dataset used in this project is a set of florescent microscopic images, which is not monochromic. Furthermore, nucleus and membrane are distinguished using blue and green colors.

Other than accurate cell segmentation, the benefits of using this framework can also be noted as the following :

1. Scalability: The probabilistic deformable model for each cell can be applied on an image with several cells by employing the approximate window technique discussed.

2. Parallelizable: Since the segmentation algorithm is applied on each approximate window separately, different windows can be processed in a parallel manner in order to reduce the running time of cell segmentation on the whole image.

We use our approach to study the cell morphology as outcome of a growth factor (cytokine) delivery procedure.

Our future work includes the integration of our framework into a unified optimization approach, where classification and deformable model parameters will be estimated using an L1-norm logistic classication in a Max-product procedure.

LIST OF REFERENCES

LIST OF REFERENCES

[1] X. Wang, W. He, D. Metaxas, R. Mathew, and E. White. Cell segmentation and tracking using texture-adaptive snakes. In *Biomedical Imaging: From Nano to Macro, 2007. ISBI 2007. 4th IEEE International Symposium on*, pages 101–104, april 2007.

[2] W. He, X. Wang, D. Metaxas, R. Mathew, and E. White. Cell segmentation for division rate estimation in computerized video time-lapse microscopy. *Multimodal Biomedical Imaging II*, 6431(1):643109, 2007.

[3] Y. Freund and R. E. Schapire. A decision-theoretic generalization of on-line learning and an application to boosting. In *Proceedings of the Second European Conference on Computational Learning Theory*, EuroCOLT '95, pages 23–37, London, UK, UK, 1995. Springer-Verlag.

[4] C. Cortes and V. Vapnik. Support-vector networks. *Machine Learning*, 20:273–297, 1995.

[5] S. Beucher and C. Lantuejoul. Real-time edge and motion detection/estimation. In *International Workshop on Image Processing, Rennes, France*, sep. 1979.

[6] R. Ali, M. Gooding, M. Christlieb, and M. Brady. Advanced phase-based segmentation of multiple cells from brightfield microscopy images. In *Biomedical Imaging: From Nano to Macro, 2008. ISBI 2008. 5th IEEE International Symposium on*, pages 181–184, may 2008.

[7] S. Fitch, T. Jackson, P. Andras, and C. Robson. Unsupervised segmentation of cell nuclei using geometric models. In *Biomedical Imaging: From Nano to Macro, 2008. ISBI 2008. 5th IEEE International Symposium on*, pages 728–731, may 2008.

[8] T. Chen, Y. Zhang, C. Wang, Z. Qu, M. Cai, F. Wang, and T. Syeda-Mahmood. Local complex phase based level set and its application to dic red blood cell segmentation. In *Biomedical Imaging: From Nano to Macro, 2011 IEEE International Symposium on*, pages 187–190, april 2011.

[9] H. Layman, A. A. Rahnemai-Azar, S. M. Pham, G. Tsechpenakis, and F. M. Andreopoulos. Synergistic angiogenic effect of codelivering fibroblast growth factor 2 and granulocyte-colony stimulating factor from fibrin scaffolds and bone marrow transplantation in critical limb ischemia. *Tissue Eng Part A*, 17(1-2):243–54, 2011.

[10] N. Otsu. A threshold selection method from gray-level histograms. *IEEE Transactions on Systems, Man and Cybernetics*, 9(1):62–66, jan. 1979.

[11] T. F. Chan and L. A. Vese. Active contours without edges. *Image Processing, IEEE Transactions on*, 10(2):266–277, feb. 2001.

[12] G. Dougherty and W. Davros. Digital image processing for medical applications. *Medical Physics*, 37(2):948–949, 2010.

[13] L. G. Shapiro and G. C. Stockman. *Computer vision*. Prentice Hall, 2001.

[14] P. K. Sahoo, S. Soltani, A. K. C. Wong, and Y. C. Chen. A survey of thresholding techniques. *Comput. Vision Graph. Image Process.*, 41(2):233–260, feb. 1988.

[15] F. Benmansour, S. Bonneau, and L. D. Cohen. Finding a closed boundary by growing minimal paths from a single point on 2d or 3d images. In *Computer Vision, 2007. ICCV 2007. IEEE 11th International Conference on*, pages 1–8, oct. 2007.

[16] S. Wang, T. Kubota, J. M. Siskind, and J. Wang. Salient closed boundary extraction with ratio contour. *Pattern Analysis and Machine Intelligence, IEEE Transactions on*, 27(4):546–561, april 2005.

[17] R. Szeliski. *Computer vision: algorithms and applications*. Springer-Verlag New York, Inc., New York, NY, USA, 1st edition, 2010.

[18] Z. Yin, R. Bise, M. Chen, and T. Kanade. Cell segmentation in microscopy imagery using a bag of local bayesian classifiers. In *Biomedical Imaging: From Nano to Macro, 2010 IEEE International Symposium on*, pages 125–128, april 2010.

[19] T. McInerney and D. Terzopoulos. Deformable models in medical image analysis. In *Mathematical Methods in Biomedical Image Analysis, 1996., Proceedings of the Workshop on*, pages 171–180, june 1996.

[20] M. Kass, A. Witkin, and D. Terzopoulos. Snakes: Active contour models. *International Journal of Computer Vision*, 1:321–331, 1988.

[21] R. Szeliski. Bayesian modeling of uncertainty in low-level vision. *International Journal of Computer Vision*, 5:271–301, 1990.

[22] S. Osher and J. A. Sethian. Fronts propagating with curvature-dependent speed: Algorithms based on hamilton-jacobi formulations. *Journal of Computational Physics*, 79(1):12–49, 1988.

[23] G. Tsechpenakis. Deformable model-based medical image segmentation. In Ayman S. El-Baz, Rajendra Acharya U, Majid Mirmehdi, and Jasjit S. Suri, editors, *Multi Modality State-of-the-Art Medical Image Segmentation and Registration Methodologies*, pages 33–67. Springer US, 2011.

[24] F. Li, X. Zhou, H. Zhao, and S. Wong. Cell segmentation using front vector flow guided active contours. In Guang-Zhong Yang, David Hawkes, Daniel Rueckert, Alison Noble, and Chris Taylor, editors, *Medical Image Computing and Computer-Assisted Intervention MICCAI 2009*, volume 5762 of *Lecture Notes in Computer Science*, pages 609–616. Springer Berlin / Heidelberg, 2009.

[25] A. Gelas, K. Mosaliganti, A. Gouaillard, L. Souhait, R. Noche, N. Obholzer, and S. G. Megason. Variational level-set with gaussian shape model for cell segmentation. In *Image Processing (ICIP), 2009 16th IEEE International Conference on*, pages 1089–1092, nov. 2009.

[26] G. Tsechpenakis and D. N. Metaxas. Crf-driven implicit deformable model. In *Computer Vision and Pattern Recognition, 2007. CVPR '07. IEEE Conference on*, pages 1–8, june 2007.

[27] A. Mccallum and D. Freitag. Maximum entropy markov models for information extraction and segmentation. pages 591–598. Morgan Kaufmann, 2000.

[28] B. Zhang. Generalized k-harmonic means - boosting in unsupervised learning. Technical report, Hewlett-Packard Laboratories, oct. 2000.

[29] N. Moshtagh. Minimum volume enclosing ellipsoids. Unpublished paper.

[30] R. Huang, V. Pavlovic, and D. N. Metaxas. A graphical model framework for coupling mrfs and deformable models. In *Computer Vision and Pattern Recognition, 2004. CVPR 2004. Proceedings of the 2004 IEEE Computer Society Conference on*, volume 2, pages II–739 – II–746 Vol.2, june - july 2004.

[31] X. Fan, P. L. Bazin, and J. L. Prince. A multi-compartment segmentation framework with homeomorphic level sets. In *Computer Vision and Pattern Recognition, 2008. CVPR 2008. IEEE Conference on*, pages 1–6, june 2008.

[32] C. Saunders, M. O. Stitson, J. Weston, L. Bottou, B. Schlkopf, and A. Smola. Support vector machine – reference manual. Technical report, University of Southampton [School of Electronics and Computer Science] [http://eprints.ecs.soton.ac.uk/perl/oai2] (United Kingdom), 1998.

[33] J. C. Platt. Probabilistic outputs for support vector machines and comparisons to regularized likelihood methods. In *Advances in Large Margin Classifiers*, pages 61–74. MIT Press, 1999.

[34] J. Shi and J. Malik. Normalized cuts and image segmentation. *Pattern Analysis and Machine Intelligence, IEEE Transactions on*, 22(8):888–905, aug. 2000.